New Method for the Removal of Refraction Artifacts in Multibeam Echosounders Systems

Edouard Kammerer
John E. Hughes Clarke
Ocean Mapping Group - University of New Brunswick
Contact: kammerer@omg.unb.ca

ABSTRACT

The objective of this paper is to present a new way to process multibeam data affected by refraction artifacts. Such artifacts are often present in shallow water surveys and can very much degrade the quality of the final product if they are not addressed adequately. A perfect monitoring of the physical characteristics of the water mass would avoid the appearance of this artifact. A full control of the sound speed variations in time and space is however idealistic. This study consists of the implementation of a systematic analysis and correction software package in a post-processing context.

The methodology consists of the estimation of the variation in the water sound speed distribution by using the information given by the multibeam dataset itself. This is done by the evaluation of appropriate modelized Sound Velocity Profiles (SVP), which will be added to an already existing SVP or applied directly to the raw data. Refraction errors are most developed in the outer parts of the survey line coverage. Two methods are considered in this study: the software developed takes into account the nadir data (unaffected by refraction errors) of

- the two neighbour parallel lines and/or
- the crossing check lines

to evaluate the refraction coefficients of a two-layers SVP model that should bring the outer parts of the survey line as close as possible to the real seafloor (as observed at nadir).

The removal of such artifacts increases the useful information contained in the multibeam data. In the absence of better methods for measuring the SVP under way, this method provides an improved image of the seafloor for geoscientists and also cost effective means of handling non-critical survey projects (pipe-lines, cable route, fisheries habitats). The method also makes the results of successive survey comparisons much more meaningful.

1- INTRODUCTION

Hydrographic surveying uses sound as a remote sensing tool. Multibeam sonars are very effective tools using sound to measure depth of the ocean. The data received back by the sonar are the travel time of the signal between transmission and reflection as well as the direction from where the echo is coming back. The quality of the recovered data depends of the knowledge one has about the medium that the signal is propagating through. The wide variety of highly variable physical characteristics of the ocean makes this task a challenge. Among these characteristics, the variation of temperature, pressure and salinity affects the direction and the speed of the sound through the water. These effects are called propagation and refraction. We propose a new technique called **Ref_Clean** to improve the corrections. Its methodology of operation is first described. Then we look at its application onto a multibeam dataset.

2- NEED OF A NEW METHOD

The need for improved removal of refraction artifacts came up during the processing of two successive surveys (1993 and 1997) in the Saguenay River, (PQ, Canada). Information about the project on the Saguenay can be found in the following references: [Coté et al., 1999], [Kammerer et al., 1998], [Locat et al., 1999], [Locat et al., 1998]. Between the two surveys a catastrophic flood occurred and a huge quantity of material was eroded and brought in the fjord by the several rivers on the area. Two Digital Terrain Models (DTM) have been constituted. In order to achieve a good description of the location of the deposits, the difference between these two DTMs has been calculated. This new DTM shows two main phenomena: 1- a real changes between the two years and 2- artifacts from both surveys. Among all the artifacts revealed, refraction was the most important of all. Even after the application of the conventional methods there still often remains fairly strong artifacts. A new approach of data processing is therefore needed.

3- OVERVIEW OF THE PROJECT

The water masses vary much in space; we need to elaborate local corrections within the survey area. Refraction affects the outer beams of the swath. The central beams are much less slightly degraded. For this reason they can be used as a reference for the true depth. This method uses the nadir part of every survey line to constrain the computation of SVP corrections. Survey lines can be compared to each other in two different situations: when they are parallel to each other and when they cross each other.

In the parallel case, an appropriate SVP correction would bring the swath of the middle line in such a way that the outer parts of the swaths are merged with the outer parts of the swaths of the neighbouring lines. The nadir depths of these lines on both sides can be used as an indication of the direction that the outer parts of the swaths should take after application of the SVP correction.

In the crossing case, the nadir part of the crossing line can be used as a reference. An appropriate SVP correction deforms the swath of the line crossed in such a way that it fits with the nadir of the crossing line.

Two different approaches can be considered in order to achieve this:

The first approach consists in computing SVPs corrections to be added to the actual SVPs measured during the survey and already applied on the data. The depth and position data, provided by the sonar processing-unit, are directly used.

In the second approach, instead of using the soundings on which a SVP has already been applied, the two-way transit time and the beam angle are used to compute the synthetic SVP that removes refraction artifacts. No computation has been done on this data. A flat "neutral" SVP (with a sound speed of 1500m/s) is applied to the range and angle data. The heave of the vessel needs to be added to the depth obtained with the water column of 1500m/s. This data is processed in the same way as in the first approach.

4- METHODOLOGY

4.1 PRELIMINARY COMPUTATIONS: EXTRACTION_OMG

This project uses the multibeam processing tools developed by the Ocean Mapping Group (OMG). This software package (***SwathEd***) has its own data format [Hughes Clarke, 1999b]. The multibeam data must have already been processed with these tools when the application of **Ref_Clean** can be considered (a step taken only if refraction artifacts are still apparent in the seafloor images). The first step to be done before the application of **Ref_Clean** is the extraction of the specific data needed from the OMG processed files. A program (***extraction_OMG***) achieves this.

4.2 FIRST APPROACH: ADJUSTMENT OF THE EXISTING SVP

The purpose of this approach is to determine an additional SVP, which will remove as effectively as possible the residual refraction artifact. As the water masses tend to vary significantly in space, we need to calculate local corrections at different points along each of the survey lines. To achieve this, we apply artificial two layers step SVPs. The beams around nadir of the survey lines are used as references to give an indication of the true bathymetric surface. This approach uses the information from the two parallel lines and from crossing lines to constrain the shape of the swath of the middle line. The shape of the swath free of refraction artifact should align with the nadir depths of other surrounding lines.

4.3 SECOND APPROACH: PRELIMINARY COMPUTATIONS

In the second approach, instead of using the depth and across-track data computed with the measured sound speed, we use the transit time of the acoustic signal and the angle of the received beam. The idea is to generate synthetic two-layer SVPs that are not only corrections without any intrinsic physical meaning. Since the method needs depth and across-track values in input, the time and angle data are converted into depth and across-track. A sound speed value describing a homogeneous "neutral" water column is chosen to perform this computation. The global average sound speed value throughout the oceans is 1500 m/s. The heave of the ship is added to the depth.

Eq. 1 $$d = 1500.\Delta t.\cos(\theta) + h \qquad a = 1500.\Delta t.\sin(\theta)$$

Here d is the depth, a the across-track value, Δt the transit travel time, θ the beam angle and h the heave value.

After these computations the methodology is identical to that of the first approach. The difference stands in the actual meaning of the results obtained. The results of the second approach are the corrections to be added if the water masses had previously a fictitious homogeneous average value of 1500m/s. They have then connections with the actual physical sound speed distribution through out the area.

4.4 CASE OF PARALLEL LINES.

4.4.1 First step: decomposition of the survey line into small datasets

The program called ***para1_find*** receives in input the files created by ***extraction_OMG*** for each of the three parallel survey lines. The purpose of the decomposition is to breakdown the three lines into a series of blocks of equal length. Each block contains three segments of line of the three lines considered. To achieve this, we project the navigation of the three lines on an imaginary straight line aligned along the average of the headings of the three lines. We select the area where this straight line has a neighbouring line on both sides. The two black dots in the Figure 1 are the ends of the selected area. The line is cut in a certain number of segments of equal length.

From the data of each segment the following values are extracted or computed: 1- The ping number in the middle of the segment for the each line, 2- The average nadir depth for the each line (a1, a2, a3), 3- The average tide for each line (t1, t2, t3), 4- The latitude and longitude of the centre of the segment for the middle line, 5- The average distance between the navigation of each lines (d12, d23), 6- The 60 average across-track and depth values for the middle line (acc[0, ... ,59], dep[0, ... ,59]).

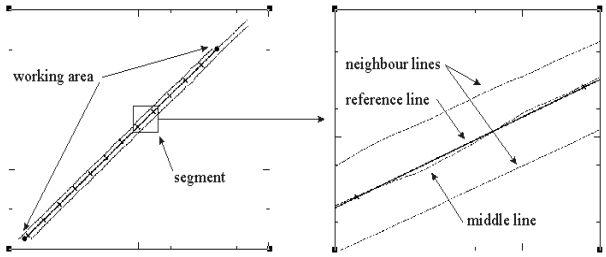

Figure 1: The figure on the left is the global view of the three survey lines, the common segment and its partition in segments. The right figure is a close-up view on one of these sub segments.

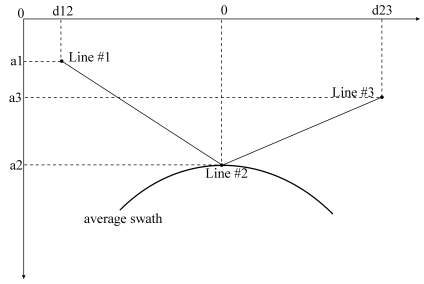

Figure 2: relative position of the different lines in a cross section of each segment. First method above: the swath is adjusted to the nadir depth of the line #2.

4.4.2 Second step: Adjustment of the Average Swath:

The program called ***para2_adjust*** realizes this step. From the data computed in the previous paragraph (§4.4.1), we proceed now to the evaluation of the SVP that brings the average swath as close as possible to the two lines joining the nadirs (see Figure 2). This is done individually in each segment. The first step is to reduce the average nadir depths of each line with the tide coefficients computed above:

Eq. 2 $$a1=a1+t1,\ a2=a2+t2,\ a3=a3+t3$$

The sixty beams of the average swath of the middle line are then shifted vertically in order to have at the same level the average nadir depth and the average of the twenty central beams.

Eq. 3 $$depth[i] = depth[i] + a2 - \frac{1}{20}.\sum_{i=20}^{40} depth[i]$$

At this point, the optimization of the refraction coefficient can now be carried out (see §4.8).

4.5 CASE OF CROSSING CHECK-LINES.

The idea developed in the case of crossing lines is to use the nadir beams of the check-line. It is used as a reference for the true shape of the seafloor in order to estimate the refraction coefficients that bring the average shape of the swaths of the line being analyzed as close as possible to this reference profile.

4.5.1 First Step: Localization of the Crossing Point.

The algorithm ***cross1_find*** determines the geographical coordinates and the ping numbers of the crossing point between the survey line and the crossing check-line.

First, from the boundary files it determines if the two boundary boxes overlap. If they do intersect and if the difference in heading between the two crossing lines is large enough (intersection angle within ±30° from the orthogonal), the program reads the navigation files and looks for the intersection point between them. In order to do this, it looks for the minimum distance between the middle of segments constituted by two navigation points of each line (see Figure 3 below). The exact location of this intersection is determined by computing the equations of the two straight lines passing by the four navigation points of the two segments giving the minimum distance.

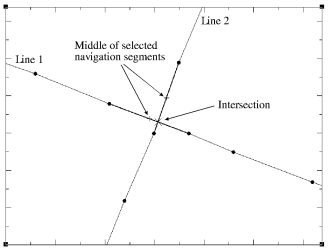

Figure 3: Schema of an intersection between two survey lines.

*4.5.2 Second Step: Selection of the Data to Compare.(realized by **cross2_grid**)*

Selection of the data from the survey line: From the survey line we select a certain number of profiles on each side of the intersection location determined in the first step. These profiles are averaged in latitude, longitude, across-track and depth. This average profile is our information about the survey line in the area. The averaging tends to weaken the influence of real features on the seafloor and to keep only the refraction artifact and the natural slope. The Figure 4-Left below shows the profiles selected from the survey line on both sides of the intersection point.

Selection from the check-line: From the check-line only the nadir part is interesting us. In order to avoid the influence of spikes (penetration and amplitude/phase transition area noise) and real features on the sea bottom, the data (latitude, longitude, across-track, depth) from the 10 central beams of 200 swaths are averaged out. The Figure 4-Right below shows the average of the 10 beams around nadir selected from the check-line on both sides of the intersection point.

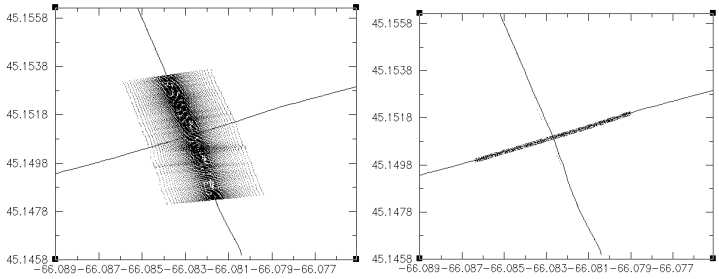

Figure 4: Left: Selection of 200 profiles from the survey line on both sides of the intersection point with a check-line. Right: Selection of the nine beams around the nadir of the check-line.

Projection of the two selections on a common straight line: To be compared, these two profiles are projected on a reference straight line defined by the average heading of the pings selected out of the check-line and which goes through the intersection point. The Figure 5 below shows the superposition of the two average profiles on the reference straight line.

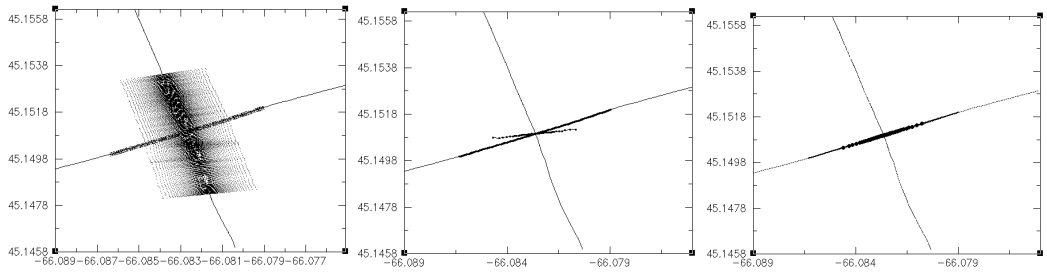

Figure 5: Left: view of the selections made from the two crossing lines. Centre: average profiles of the swaths of the survey line and the central beams of the check-line. Right: The average profiles are projected on the line defined by the average heading of the check-line at this location.

*4.5.3 Third Step: Comparison of the Two Average Profiles. (realized by **cross3_adjust**.)*

Resampling of the survey line average profile: Having averaged 200 swaths from the survey line, we now have a profile of 60 beams (for a Simrad EM1000). We averaged 10 central beams from 200 swaths of the crossing line, from which we generated another profile but this time of 200 points. In order to compare these two datasets we resample the points from the crossing line (200 points) onto the equivalent positions of the beams of the survey line profile (60 points). The profile of the crossing line obtained is shifted vertically so that its nadir beams are at the depth of the other profile (the shift corresponds to the average vertical error present in the dataset (see §4.9 for external errors)). The profile obtained with the survey line profile is plot on the Figure 6-Left:

Computation of the trend of the crossing line profile: The trend of the nadir profile of the crossing line is computed and plotted in the Figure 6-Centre below.

Computation of the refraction coefficients: The search algorithm is described in §4.7. The coefficients of the two-layers SVP are computed in order to minimize the distance between the two profiles. The criterion used is the sum of the squares of the vertical differences between the survey line average swath and the trend of the crossing line profile. This brings the average swath of the survey line the closest possible to the trend of the crossing line profile. The Figure 6-Right below illustrates this. Notice the slight roll bias between the deformed swath and the trend of the crossing line.

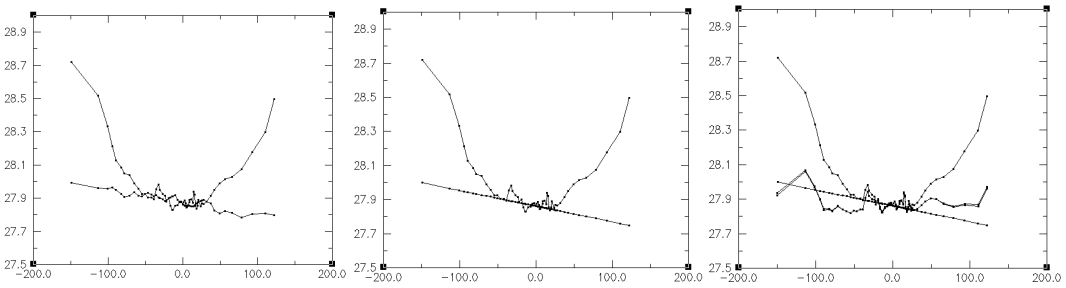

Figure 6: Left: Superposition of the profile from the survey line (the curved profile) with the gridded profile from the crossing line. Center: Comparison between the trend of the crossing line profile and the survey line average swath. Right: Plot of the survey line average swath deformed by the two-layer SVP solution of the optimization algorithm.

4.6 ROUGHNESS OF THE SEAFLOOR

Even with the average calculated in the two methods described above, the natural morphology of the seafloor sometimes still appears in the profile used to determine the refraction coefficients. This happens if there is significant topography of length scales at about the dimension of the number of pings used for the average. It biases the computations. To prevent this from happening, we estimate the roughness of the area and weight the refraction coefficients according to this roughness. Refraction artifacts are usually highly visible in flat and monotonous terrain and much less visible in rough topography zones.

The roughness is defined in an area by two different components. The first component is called the across-track roughness; it is determined from the average profile in a segment of the survey line. The second component is the along-track roughness; it is the roughness of the nadir area along the survey line.

4.6.1 Across-track Roughness

The across-track roughness is computed from the average profile in each segment of the survey line and at the crossing points of two lines. The coefficients of a best fitting parabola of the average profile are computed (Figure 7). Such a parabola is not symmetric on the *y*-axis because of the natural slope is included in the data.

The roughness *r* of the average profile is defined as the sum of the square of the differences between the best fitting parabola $d_{parabola}$ and the average depths d_{ave} computed for the *N* beams. *r* is then divided by the number of beams *N* used. The roughness is also normalized by the average nadir depth $\bar{z}$ to make it independent of the depth of the area where it is computed.

Eq. 4

$$r_{across} = \frac{\sqrt{\sum_{0}^{N} \left(d_{ave} - d_{parabola}\right)^2}}{N.\bar{z}}$$

What we consider as roughness here is in fact the average of the residuals of a second-degree approximation of the across-track profile. The shape of the refraction artifacts is very similar to the shape of a parabola. The result of the roughness computation is then independent of refraction artifacts

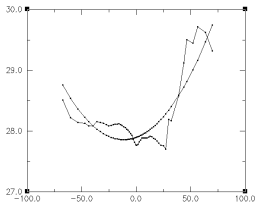

Figure 7: average profile of a segment of a survey line with the best fitting parabola

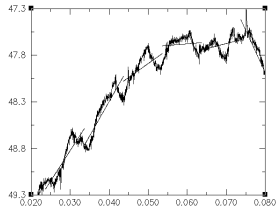

Figure 8: part of the depth profile of a survey line with the best fitting straight lines for every segments.

4.6.2 Along-track Roughness

The along-track roughness describes the roughness in the nadir part of the stripe of seafloor ensonified in an along track direction. This computation is realized in each segment of the survey line. For each ping in the segment, the depths of the central beams are averaged out. The position of the resulting depth is computed as the distance from the coordinates of the nadir beam of the current ping to the coordinates of the first ping of the line. We have thus a series of couples (depth, distance). The trend of this depth series is computed. The roughness is the sum of the squares of the differences between the averaged nadir depth and the value of the trend at this position. The formula for this computation is shown below with d_{nadir} the average nadir depth, d_{trend} the depth of the trend and *N* the number of pings in the line segment, as the across-track roughness it is normalized by the average nadir depth $\bar{z}$:

Eq. 5

$$r_{along} = \frac{\sqrt{\sum_{0}^{N} \left(d_{nadir} - d_{trend}\right)^2}}{N.\bar{z}}$$

4.6.3 Weighting of the Refraction Coefficients

The final roughness *r* used is the average of the across-track and along-track roughness. The refraction coefficients are weighted accordingly to the roughness computed. A null roughness let the refraction coefficients unchanged. The greater the roughness the less efficient the method would be, the more the refraction coefficient should be reduced. The weighting function below fulfills these two conditions:

Eq. 6

$$\Delta c_{new} = \Delta c_{old} \cdot \frac{1}{1 + a.r}$$

The positive constant a is determined depending of how strong the weighting is wished to be. The choice of a is up to the user, he chooses it accordingly to the kind of topography present in the area. In the presence of very rough local topography a high value of a should be chosen so as soon as the roughness increases the weighting will strongly reduce the amplitude of the coefficients. In the presence of flat and monotonous area with long wavelength topography a small value of a can be chosen. This weighting is applied to both the surface sound speed discontinuity $\Delta c=c_0-c_1$ and the discontinuity between the two layers at the depth z_s, $\Delta c=c_2-c_1$ (c_1 is constant).

4.7 Search of the Refraction Coefficients

This section is common for the two cases of parallel lines and crossing lines. It is repeated successively in the different segments designed and once at the intersection between two crossing lines.

Once the first computations are done the search of SVP coefficients starts. The correction sought has the form of a two layer artificial SVP. It can be proved that the width z_s of the discontinuity layer, the velocity of the first layer c_1 and the velocity of the second layer c_2 are dependant variables. Therefore if we fix the depth of the discontinuity z_s and the sound speed of the first layer c_1, the only variables that we look for are c_2 and c_0.

Parallel lines case: We are looking for a SVP which brings the swath of line #2 as close as possible to the two segments of line joining the nadir of the two neighbouring lines. The function on which the search is based is then the sum of the square of the differences between the swath and these two segments of line. A minimum of this function is sought. The SVP coefficients bringing the function to its minimum constitute the SVP correction.

Crossing lines case: We are looking for a two layer SVP that brings the survey line averaged swath as close as possible to the nadir profile of the crossing line. The function used in this case is the sum of the squares of the differences between the trend of the nadir profile of the crossing line and the survey line average swath. One projected onto the other.

In order to find these minimums, the Fibonacci search algorithm is used [Cheney, 1980]. This algorithm looks for the minimum of a continuous function f in an interval [a, b]. It is used to determine c_2 and then c_0. The algorithm compares the values of the function at one third and two third of the interval [a, b] between themselves. The interval is reduced by one third of its length on the side of the highest value of the function found. After a certain number of iterations the length of the interval is considered small enough to give a good accuracy of the minimum which is then taken in the middle of the interval.

4.8 Final Computations

For each segment of a survey line flanked by two other lines and for each intersection point between two lines the Ref_Clean package generates a two-layer SVP solution. The two coefficients of the SVPs from a line are stored in specific file. The refraction tool holds the last coefficients constant to the ends of line. A flat SVP (c_0=1500m/s, c_2=1500m/s) is put automatically at the first and at the last ping number of the line in order to smooth down the corrections at the extremities of the line. The end of lines are subject to motion sensor problems that induces in the data gross roll biases and long period heave errors, which makes any attempt of refraction artifact removal pointless and possibly misleading (see External Errors in the §4.9).

Such a refraction coefficient file is generated for every survey line. These files are then used with the OMG software (***weigh_grid***) that is used to apply these coefficients and to grid the dataset in order to create a DTM of the data.

4.9 External Error Sources

There are a series of errors that are external to the refraction problems which sometimes affects multibeam soundings. In this section we look at the consequences of the presence of such errors on the application of the method proposed here. We distinguish the vertical and rotational errors.

4.9.1 Vertical Errors

Different kinds of vertical errors can be present in multibeam soundings. It can be an imperfect tidal reduction or problems with long period heave. These errors induce an erroneous vertical displacement of the swath.

For the **parallel lines** comparison, the vertical displacement is present in the average nadir depth computed in each segment. After processing, this false step is smoothed but is still present. This will result in an inappropriate selection of refraction coefficients.

For the **crossing lines** comparison, the offset found between the two average profiles gives an estimation of the vertical error present (see §4.5.3). The two profiles are brought together for the estimation of the refraction coefficient. The vertical error due to tide imperfections then does not interfere during the application of the refraction removal method. It stays in the processed data as it was before processing.

4.9.2 Rotational Errors

Roll bias is also sometimes present in multibeam data. It occurs under different circumstances such as after an imperfect patch test or during and after a strong turn of the vessel with a motion sensor that does not account properly for lateral accelerations. It can be observed as a tilt of the swath with respect to the neighbour lines. One end of the swath is higher than the end of the neighbouring swath and the other end lower (see Figure 9). It is a big hindrance towards the success of the method because the roll error is not symmetric with respect to the vertical axes at nadir. A SVP application symmetrically affects both sides of the swath, and thus no refraction adjustment can make the swath fitting with its neighbours. The presence of roll bias prevents the method operating correctly.

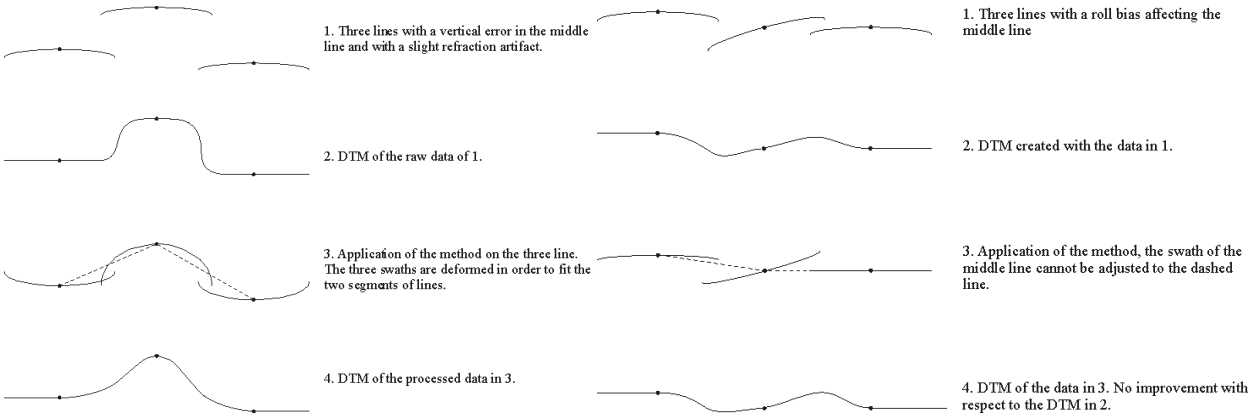

Figure 9: Effect of the application of the proposed method onto a line affected by a vertical offset (on the left: the method smoothes the step but does not remove it) and by a roll offset (on the right: the method is inefficient to perform correctly in this case).

5- RESULTS AND ANALYSIS

5.1 PRESENTATION OF THE DATASET USED

In this part, the method described above in §4- is applied on a real multibeam dataset. The survey chosen has been carried out for the Canadian Hydrographic Service in the approaches of the St John harbour (New Brunswick) in June 1994. The multibeam echosounder used is an EM1000 from Simrad [Simrad, 1992]. It is mounted on the hull of the SWATH vessel CSS Frederick G. Creed. The area is rather shallow; the seafloor lies below 10 to 60 meters of water. A sun illumination of the DTM is presented on the Figure 10 below. The topography is relatively flat except for one major rock outcrop (on the upper right hand side North East corner). The refraction artifacts that corrupt the dataset appear very clearly under the shape of long stripes in the overlapping areas between the survey lines.

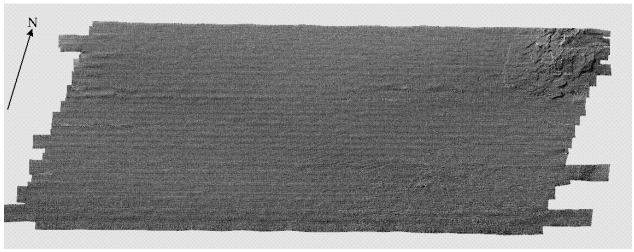

Figure 10: Multibeam survey off Saint John (NB) harbour (CHS, Simrad EM1000, June 1994). This picture shows the data without any refraction post-processing. Note the refraction artifact (stripes parallel to the survey lines).

5.2 APPLICATION OF THE METHOD

First, with the program ***extraction_OMG*** (see §4.1), the data files of the survey lines are converted into the **Ref_Clean** format. This operation creates three files for each survey data file: a bathymetric file, a navigation file and a boundary file. From these files we are now ready to proceed to the refraction coefficients estimation.

As described in the §4.4 each survey line is decomposed in segments having two parallel segments on each side. The center of each of these segments can be seen on the Figure 11 below with the navigation.

As described in the §4.5 the algorithm looks for the intersections of every check-line with all the survey lines. The intersection points found can be seen on the Figure 11 below.

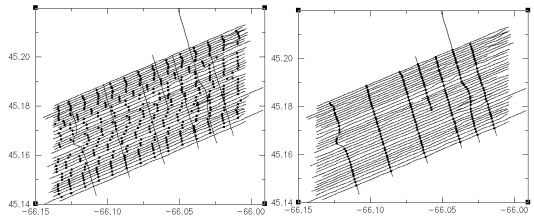

Figure 11: Navigation of Saint John dataset. The black dots are the centre of segments of the survey lines (left) and intersections between parallel survey lines and crossing check-lines (right).

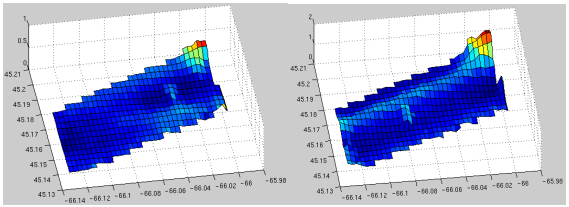

Figure 12: 3d graph of the gridded geographic distribution of the across-track roughness (left) and along-track roughness(right) for each segment of the survey lines.

5.2.1 Computation of the Roughness

As explained in the §4.6, the refraction coefficients are weighted with a roughness coefficient. The Figure 12 below shows the across-track and along-track roughness grids. Notice the peak of roughness at the North-East corner of the area on both grids. It corresponds to the rock outcrop that shows up on the DTM in the Figure 10.

It has to be noticed also on this picture a high along-track roughness region parallel to the direction of the survey lines. It covers the area mapped by the survey lines done during the 7th of June. The heave this day was stronger this day and probably due to imperfections in the motion sensor, introduced artifacts in the multibeam data. There is then less confidence in the data and an appropriate weight on the SVP correction is then justified. The two sets of coefficients are averaged to obtain the final coefficients used to weight the application of the SVP correction.

5.2.2 Refraction Coefficients

As explained in §4.8, this operation generates for each survey line a file of refraction coefficients. The results in surface sound speed c_0 and in the sound speed c_2 of the second layer of the synthetical SVP are displayed for the two different approaches in the four graphs below:

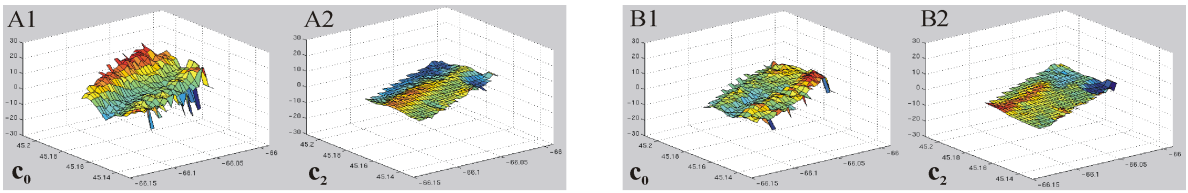

Figure 13: geo-distribution of the surface sound speed c_0 (left) and the sound speed c_2 of the second layer (right), corrections to the actual SVPs.

The values of surface sound speed c_0 have much larger variations in amplitude than the values of c_2. The four graphs have the same scale; the 3D graphs of c_2 appear very flat compare to the graphs of c_0.

In the correction values of c_2, two different zones can be distinguished in the Figure 13-A2: a zone of negative c_2 for the 7 most northern lines. All these lines have been run during the first day of the survey, the 6th of June. The rest of the nodes have positive values.

5.3 RESULTS

Three DTMs are created with these refraction coefficients. The first DTM is created with the initial survey SVPs. The second DTM is made with the same data but with the refraction correction coefficients computed with the first approach of the **Ref_Clean** tool. The third DTM is realized from the files created with a "neutral" 1500 m/s SVP on which the refraction coefficients computed with the second approach of **Ref_Clean** are applied. To have a better understanding of the impact of the method onto the data a profile is also taken and analyzed. In this section we compare these three DTMs and the profiles for the different approaches.

5.3.1 *DTM comparison*

The DTMs are decomposed in three parts in order to have a closer look to the results of the Ref_Clean tool. The middle part is shown below in the Figure 14. This picture is in fact a sun illumination of the DTMs. The azimuth in which the sun illuminates the data has been chosen orthogonal to the direction of the parallel lines in order to emphasize the relief parallel to the survey lines (such as refraction artifacts).

On this picture, it can be noticed that the **Ref_Clean** tool operates correctly and remove the long stripes that appear in the overlapping areas of the survey lines in the top parts of the three figures.

However a few remarks need to be made about these pictures:

1- Notice that some artifacts still appear at the extremities of the survey lines. These artifacts are not refraction artifacts but cornering effects due to an imperfect motion sensor, which needs a certain delay of time to settle down after the strong motions involved during the turn just achieved.

2- As well some local artifacts seem to stay after applying the method at different places in the area. These artifacts are due to imperfections of the motion sensor. It is sensitive to turns made by the helmsman to correct a distance taken by the ship from the straight planned survey line (like avoiding a buoy).

These two phenomenon are described in detail in the next section (see §5.4).

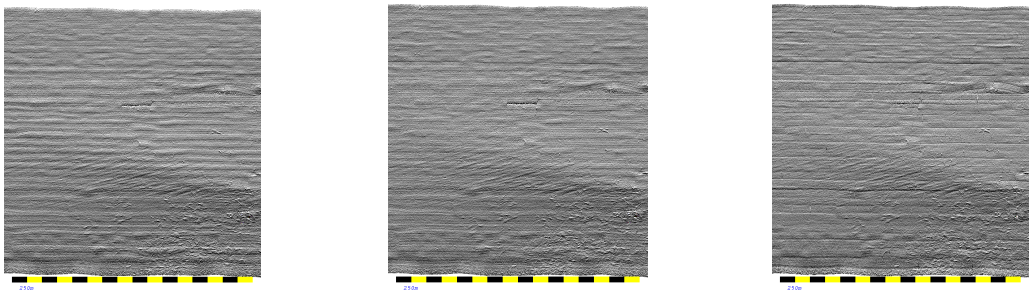

Figure 14: Results for the central part of the survey area. Left: initial data with the actual SVPs taken during the survey. Center: results of the first approach (corrected SVPs). Right: results of the second approach (new SVPs).

5.3.2 Profile comparisons

Three different profiles are taken orthogonally to the parallel lines at different depths. These profiles show, in an even closer way than with the DTMs, the effects of the **Ref_Clean** tool onto the shape of the swaths. One can notice from these three figures that the **Ref_Clean** tool flattens the across-track profiles of the survey lines to make then aligned with each other resolving by this way the refraction problems. The shallowest profile (Figure 15-Left) presents upward refraction artifacts when the two other profiles have rather downward refraction artifacts. It can be seen on these figures that when a roll bias or a depth error affects the survey line the application of **Ref_Clean** does not improve the situation. (see External Errors §4.9).

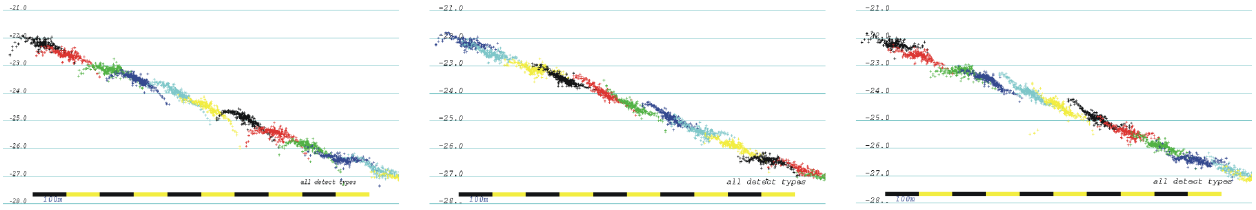

Profile with actual SVPs | Profile with corrected SVPs | Profile with new SVPs

*Figure 15: Result of the two method of application of the **Ref_Clean** tool. Left: data with real SVPs, centre: data after correction of the SVP, right: data with new SVP from transit time and beam angle.*

5.4 ANALYSIS

5.4.1 Cornering effects

The echosounder EM1000 used for this survey was interfaced with a TSS 335B motion sensor. This instrument provides to the echosounder the motion attitude of the vessel (i.e. roll, pitch, heave and gyro). An investigation of the roll and heave errors present in the Frederick G. Creed – EM1000 when using a TSS-335B motion sensor [Hughes Clarke, 1993] reveals that at the surveying speed of 16 knots:
1/ the vessel after completion of a turn needs 3 minutes prior to start of line to be steady on course
2/ and it requires an extremely gentle line keeping.

In the dataset of St John harbour, such roll and heave biases are observed at the start of the survey lines. The Figure 16 shows two profiles taken across a few lines at each extremities of the area. In the profile #1 on the left a few lines are alternatively one metre above and one metre below its neighbour. It shows that these lines are affected by a heave bias of approximately one metre. In the profile #2 a few lines show a roll bias rather pronounced.

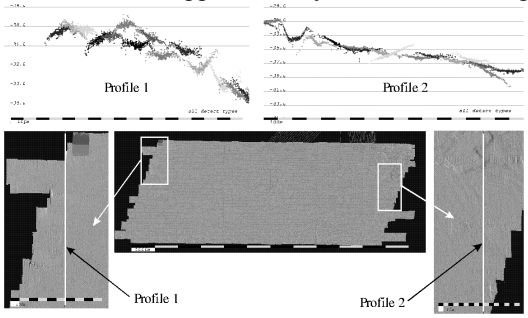

Figure 16: Roll and heave biases occurring at the extremities of the survey lines.

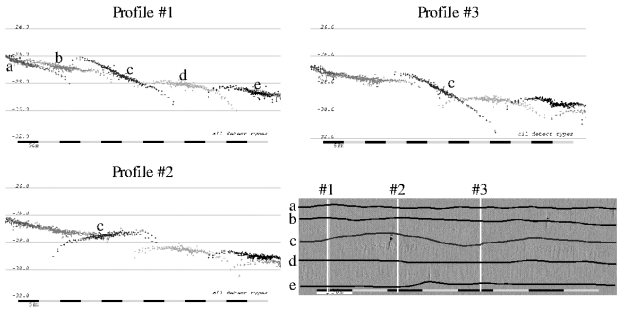

Figure 17: Roll bias occurring within a survey line when the vessel slides away from a straight navigation.

5.4.2 Local roll artifacts

The second recommendation from [Hughes Clarke, 1993] about an extremely gentle line keeping is also justified. When the vessel is taken away from a straight navigation and executes long period maneuvers a roll bias is induced in the data. In the St John dataset this event occurred on several occasions. A closer look onto the data

shows the roll bias that has been induced. See on Figure 17 the example where the vessel has realized an oscillation around a straight line. Three profiles show that a roll bias follows the oscillation of the ship.

6- CONCLUSION

Refraction artifacts, like other artifacts, degrade the results of hydrographic surveys. The removal of such artifacts increases the information brought by the multibeam data. In the absence of better method measuring the SVP under way, it would provide a better imagery of the seafloor that geoscientists are looking for and be cost effective means of handling non-critical survey projects (pipe-lines, cable route, fisheries habitats). Perhaps with appropriate caveats (200% coverage and a large enough number of check lines) this can be accepted for rigorous hydrographic surveys. The objective of this research is to provide a good tool capable of reducing the impact of refraction artifacts on multibeam data. It will make the results of successive survey comparisons much more readable.

References and Bibliography

Cheney, W., D. Kincaid (1980). *Numerical Mathematics and Computing*; second ed., Brooks/Coles Publishing Company.

Coté, P., Maurice, F., Kammerer, E., Hill, P., Locat, P., Simpkin, P., Long, B., Leroueil, S. (1999). *Intégration des methodes géotechniques et géophysiques pour le calcul du volume des sédiments de la couche de 1996 dans la baie des Ha!Ha!*. Comptes Rendus du congrès à Montréal de SCMO. p.138.

Hughes Clarke, J.E. and Godin, A., (1993). *Investigation of the roll and heave errors present in Frederick G.Creed - EM1000 data when using a TSS-335B motion sensor*, DFO Contract Report FP707-3-5731.

Hughes Clarke, J.E (1999b), SwathEd, http://www.omg.unb.ca/~jhc/SwathEd.html

Kammerer, E., Hughes Clarke, J.E. (1998). *Monitoring temporal changes in seabed morphology and composition using multibeam sonars: a case study of the 1996 Saguenay River floods*, Proceedings of the Canadian Hydrographic Conference 1998, Victoria, pp. 450-461.

Locat, J., Mayer, L., Gardner, J., Lee, H., Kammerer, E., and Doucet, N., (1999). *The use of multibeam surveys for submarine landslide investigations*. Invited paper. International Symposium on: Slope Stability Engineering: Geotechnical and Geoenvironmental Aspects, Shikoku, 8 p., in press.

Locat, J., Kammerer, E., Doucet, N., Hughes Clarke, J., Mayer, L.et al. (1998). *Comparaison des sondages multifaisceaux réalisés en 193 et 1997 dans la partie amont du fjord du Saguenay : analyse préliminaire de la couche de 1996 et d'éléments géomorphologiques* : Comptes rendus du Congres de l'Association Géologique Canadienne à Québec.